Journal of Solid State Chemistry 184 (2011) 871–876

Contents lists available at ScienceDirect

Journal of Solid State Chemistry

journal homepage: www.elsevier.com/locate/jssc

Microstructure and magnetic properties of electrospun one-dimensional Al^{3+}-substituted $SrFe_{12}O_{19}$ nanofibers

Mingquan Liu, Xiangqian Shen*, Fuzhan Song, Jun Xiang, Xianfeng Meng

School of Materials Science and Engineering, Jiangsu University, Zhenjiang 212013, PR China

ARTICLE INFO

Article history:
Received 11 August 2010
Received in revised form
16 January 2011
Accepted 11 February 2011
Available online 23 February 2011

Keywords:
Strontium ferrite
Substitution
Nanofibers
Microstructure
Magnetic properties

ABSTRACT

$SrAl_xFe_{12-x}O_{19}$ (x=0–3.0) nanofibers with diameters about 100 nm have been prepared by electrospinning and subsequent heat treatment. With Al^{3+} ion content ranging from 0 to 3.0, the lattice parameters decrease due to Fe^{3+} ions substituted by smaller Al^{3+} ions and the average grain size calculated by the Scherrer's equation reduces from 65 to 37 nm. The magnetization shows a continuous reduction with the Al content and its value measured at 77 K is higher than at room temperature, which can be explained by Bloch's law. For the coercivity, its value initially increases, reaching a maximum value of 617 (298 K) and 547 kA m^{-1} (77 K) at x=2.0, and then reduces with the Al content further increase largely arising from the substituted Al^{3+} ion arrangement in different interstitial sites of the strontium ferrite unit cell.

1. Introduction

Hexagonal ferrites such as strontium ferrite ($SrFe_{12}O_{19}$) are of a great interest for microwave devices and millimeter-wave absorbers because of their large uniaxial magnetocrystalline anisotropy, high permeability and low conductive losses [1–3]. In order to tune the magnetic properties and ferromagnetic resonant frequency of the pure M-type ferrites, various substitutions were investigated based on the fact that their structure and ferromagnetic resonant frequency are closely related to the chemical composition and the arrangement of ions in the crystal unit [4]. Single- and multi-ions substitution such as La^{3+} [2], Cr^{3+} [4], Al^{3+} [4,5], La–Zn [6], Mn–Ti [7], Mn–Co–Zr [8], etc., were used to tailor the magnetic parameters and electromagnetic characteristics. Among these substitution ions, as Al^{3+} ions can replace Fe^{3+} ions of the strontium ferrite in any proportion [9], and have a great effect on the anisotropy field (H_A) and the ferromagnetic resonant frequency ($f \propto H_A$, where f is the ferromagnetic resonant frequency) [4], researches have been carried out to examine the effect of Al^{3+} ion substitution on the M-type ferrite electromagnetic characteristics [4,5,9].

Up to now, the reported nanostructures of Al^{3+} ions substituted M-type ferrite were focused on nanoparticles [9,10] and nano-films [11,12], but one-dimensional (1D) nanofibers have not been reported. Due to a high aspect ratio (length to diameter ratio) and anisotropy characteristics, a large surface-to-volume ratio, 1D materials can be used in many technological fields including advanced catalysts, sensors, electronics and photonics [13]. In order to obtain these 1D materials, various preparation methods have been developed such as laser ablation [14], template [15], precursor thermal decomposition [16] and electrospinning [17].Compared to other processes, the electrospinning has proved to be a versatile and effective technology for fabricating microscale and nanoscale fibers [18], in particular, for nanofibers with a complex compound and composite nanofibers. The nanofibers of various types of materials including polymers [19], metal oxides [18], and composite (organic/inorganic) [20] nanofibers have been prepared via electrospinning. Based on our previous investigation for the pure strontium ferrite nanofibers [21], the present work reported preparation of the Al^{3+} ions substituted strontium ferrite nanofibers using the sol–gel assisted electrospinning, the effect of Al^{3+} ion substitution on the microstructure, morphology and magnetic properties of the resultant $SrAl_xFe_{12-x}O_{19}$ ($0 \le x \le 3.0$) nanofibers.

2. Experimental

The preparation of $SrAl_xFe_{12-x}O_{19}$ (x=0–3.0) nanofibers was similar to the process described in our previous paper [21] and consisted of solution preparation, electrospinning and calcination. In a typical procedure, 0.5 g poly (vinyl pyrrolidone) (PVP, Mw=1,300,000, Aldrich) was dissolved in mixture of ethanol (4.5 g) and distilled water (2.0 g), followed by magnetic stirring

* Corresponding author. Fax: +86 511 88791964.
E-mail address: shenxq@ujs.edu.cn (X. Shen).

0022-4596/$ - see front matter © 2011 Elsevier Inc. All rights reserved.
doi:10.1016/j.jssc.2011.02.010

for 2 h to ensure the dissolution of PVP. Then appropriate amount of strontium nitrate [$Sr(NO_3)_2$, purity ≥ 99.5%, Sinopharm Chemical Reagent Co., Ltd], aluminum nitrate [$Al(NO_3)_3 \cdot 9H_2O$, purity ≥ 99.0%, Sinopharm Chemical Reagent Co., Ltd] and ferric nitrate [$Fe(NO_3)_3 \cdot 9H_2O$, purity ≥ 98.5%, Sinopharm Chemical Reagent Co., Ltd] with a mole ratio of $1:x:12-x$ were added into the PVP–ethanol–water solution and further magnetically stirred for about 20–24 h at room temperatures to form a homogeneous viscous solution for electrospinning. The viscous solution was loaded into a plastic syringe with a stainless steel needle (d=0.9 mm). The needle used as the positive electrode was connected to a high-voltage supply and the solution was fed at a rate of 0.5 mL/h using a syringe pump during the electrospinning process. A piece of aluminum foil used as the ground collector was placed in front of the needle tip to collect the composite fibers. The distance between syringe needle tip and collector was 13 cm and the applied voltage was 15 kV. The as-spun $SrAl_xFe_{12-x}O_{19}$/PVP composite nanofibers collected were dried and calcined at 1000 °C for 2 h in ambient atmosphere to obtain the resultant nanofibers.

The X-ray diffraction (XRD) patterns were collected on a Rigaku D/max 2500PC diffractometer with Cu $K\alpha$ radiation. Fourier transform infrared spectroscopy (FT-IR) spectra of the samples (as pellets in KBr) were recorded by a Nicolet Avatar 370 spectrometer in a wavenumber range of 400–4000 cm^{-1} at a resolution of 2 cm^{-1}. Field emission scanning electron microscopy (FE-SEM, JSM-7001 F) equipped with an Oxford INCA energy dispersive X-ray (EDX) spectrometer were employed to analyze the morphology, chemical composition and microstructure of the samples. The magnetic properties of the nanofibers specimen (~3 mg enclosed in paper) were investigated at room temperature (298 K) and 77 K (in liquid nitrogen) using a vibrating sample magnetometer (VSM, HH-15).

3. Results and discussion

3.1. Formation

Fig. 1 shows FT-IR spectra of $SrAl_xFe_{12-x}O_{19}$ nanofibers calcined at 1000 °C for 2 h with different Al^{3+} ion contents. The characteristic vibration frequencies of ν_1, ν_2 and ν_3 for these nanofibers are represented in Table 1. From Fig. 1 and Table 1, all the characteristic peaks can be assigned to the M-type strontium ferrite [22]. With the

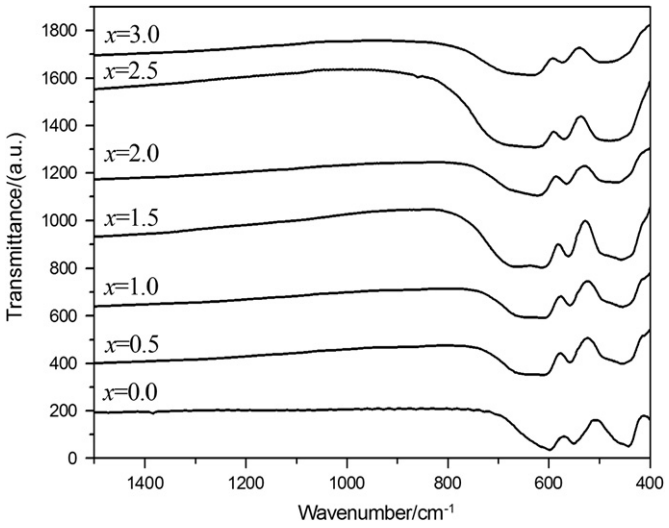

Fig. 1. FT-IR spectra of $SrAl_xFe_{12-x}O_{19}$ nanofibers with different Al^{3+} ion contents (x).

Table 1
FT-IR characteristic frequencies (ν_1, ν_2, and ν_3) and EDX elemental analysis results of as-prepared $SrAl_xFe_{12-x}O_{19}$ nanofibers calcined at 1000 °C for 2 h.

x in $SrAl_xFe_{12-x}O_{19}$	FT-IR characteristic frequencies			Elemental compositions (at%)		
	ν_1 (cm^{-1})	ν_2 (cm^{-1})	ν_3 (cm^{-1})	Sr	Al	Fe
0.0	598.0	551.8	442.3	3.2	–	37.3
0.5	607.4	556.2	448.7	3.3	1.5	34.4
1.0	611.8	559.3	455.9	3.3	3.0	35.3
1.5	617.1	561.6	458.4	3.2	4.8	33.7
2.0	623.7	564.8	466.7	3.1	6.1	31.0
2.5	627.8	570.2	477.7	3.1	7.7	29.2
3.0	631.8	572.5	491.6	3.2	9.1	27.1

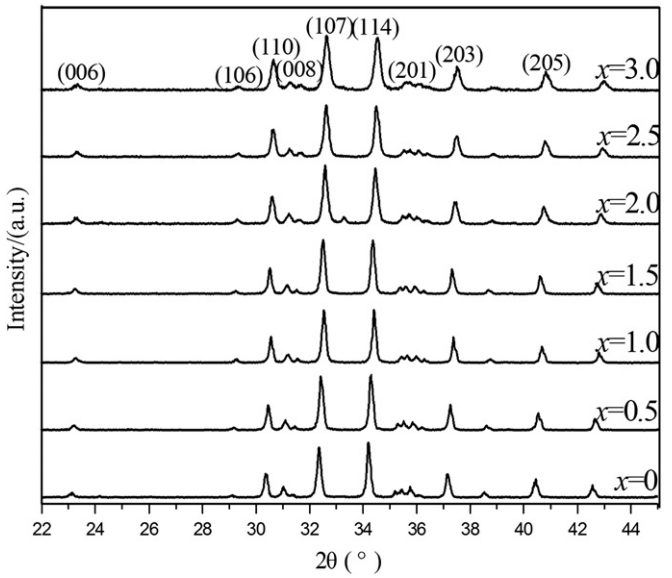

Fig. 2. XRD patterns of $SrAl_xFe_{12-x}O_{19}$ nanofibers with different Al^{3+} ion contents (x).

increase of Al^{3+} ion content, the values of ν_1, ν_2 and ν_3 shift to a higher wavenumber due to Al^{3+} ions with a lighter atomic weight than Fe^{3+} ions and the wavenumber being inversely proportional to the atomic weight [23]. It indicates that the substituted Al^{3+} ions enter the lattice.

Fig. 2 shows the XRD patterns of $SrAl_xFe_{12-x}O_{19}$ nanofibers with various Al^{3+} ion contents calcined at 1000 °C for 2 h. From Fig. 2, it can be seen that all the reflections belong to the M-type strontium ferrite (JCPDS No. 33-1340), and no other impurity phases are detected. While, with the substituted Al^{3+} ion content (x) increasing from 0 to 3.0, the reflection peaks gradually become weak and broaden, which implies the grain size becomes smaller. Comparing the reflection strength for (1 1 4) and (1 0 7) planes with the Al^{3+} ion content increased from 0 to 3.0, it can be observed that the peak strength of (1 0 7) is lower than that of (1 1 4) for the sample without Al^{3+} ion substitution, then exhibits a relative increase with the Al^{3+} ions substitution, and when the Al^{3+} ion content increased up to 3.0, it is higher than that of (1 1 4). This phenomenon can be attributed to the Al^{3+} ion substitution. It can also be seen that the diffraction peak positions for the Al^{3+} ions substituted ferrites are slightly shifted to the right of the pure strontium ferrite (x=0) as showed in Fig. 2, which is caused by the lattice constant reduction. The values of lattice parameters ($\boldsymbol{a}$) and ($\boldsymbol{c}$) obtained by fitting the diffraction peaks using the standard least-squares method are showed in Fig. 3. The lattice constants ($\boldsymbol{a}$ and $\boldsymbol{c}$) decrease with

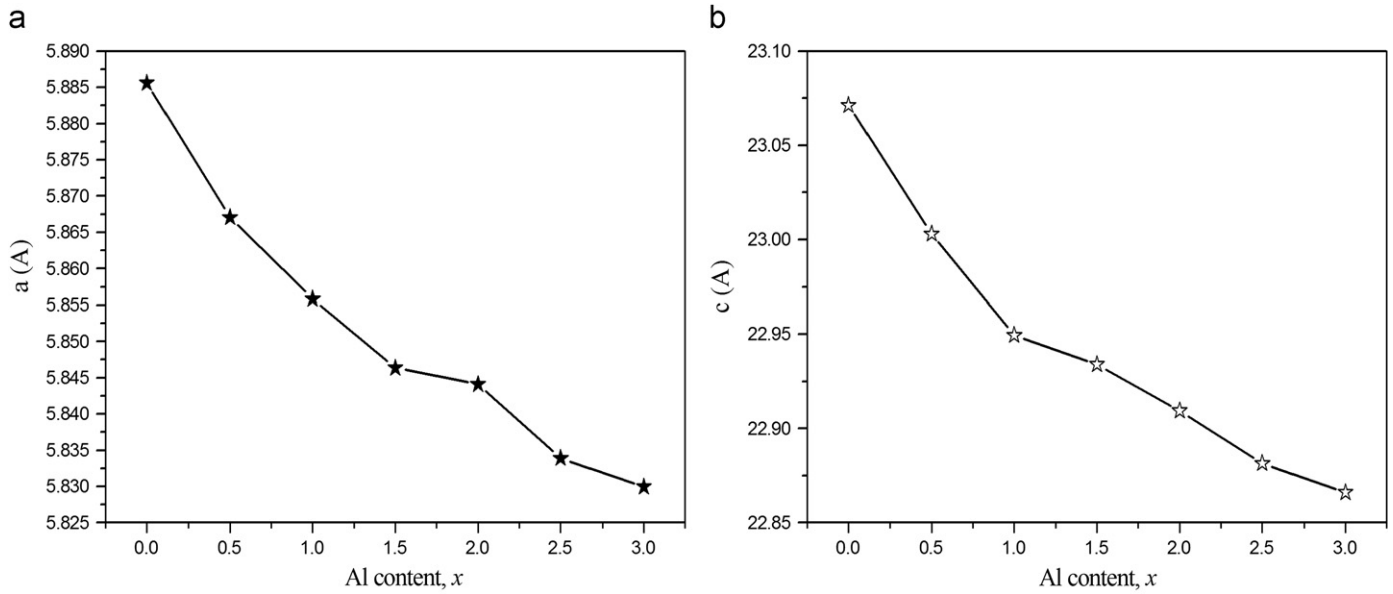

Fig. 3. Dependence of lattice constants ***a*** (a), and ***c*** (b) on different Al^{3+} ion contents (x).

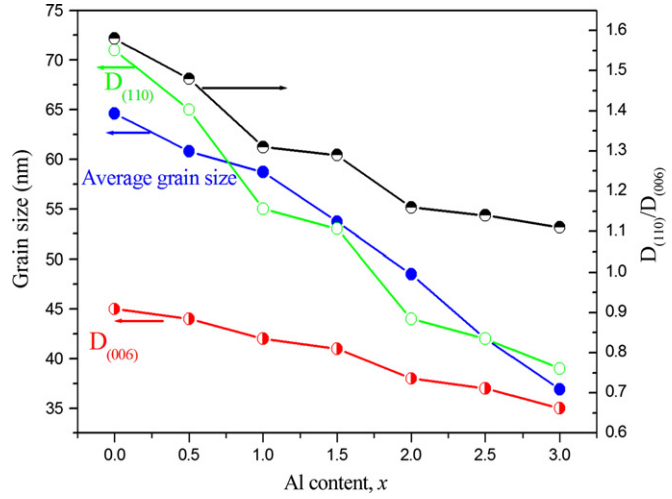

Fig. 4. Grain size of $SrAl_xFe_{12-x}O_{19}$ nanofibers with different Al^{3+} ion contents (x).

increase in x because the Al^{3+} ion radius (0.535 Å) is smaller than the Fe^{3+} ion (0.645 Å) [24].

The average grain size of $SrAl_xFe_{12-x}O_{19}$ nanofibers can be calculated from the full-width at half-maximum (FWHM) of the XRD reflection (1 0 7) and (1 1 4) planes as showed in Fig. 2 using Scherrer's equation ($D=0.9\lambda/(\beta\cos\theta)$, where λ is the wavelength of the X-ray radiation, β is the FWHM of the relevant diffraction peak and θ is the diffraction angle). The calculated grain size with the substituted Al^{3+} ion content (x) is represented in Fig. 4. From Fig. 4, it can be seen that as x increases from 0 to 3.0, the average grain size reduces from 65 to 37 nm. It is known that additives such as SiO_2, Al_2O_3, etc., are usually used to restrain the hexaferrite grain growth process due to grain boundary existences for these oxides [25]. For the ion substitution, the grain restraint mechanism should be different from the boundary effect resulting from the oxides of SiO_2, Al_2O_3, etc. As the substituted Al^{3+} ions in the lattice reduce the unit cell volume, these smaller unit cells would decrease the mass transportation among neighboring particles during the crystal growth and lead to smaller grains. Meanwhile, the grain growth orientation can be estimated referring the grain size ratio of $\boldsymbol{D}_{1\,1\,0}/\boldsymbol{D}_{0\,0\,6}$, where $\boldsymbol{D}_{1\,1\,0}$ and $\boldsymbol{D}_{0\,0\,6}$ are the calculated grain size from the plane (1 1 0) parallel to the c-axis and from the plane (0 0 6) perpendicular to the c-axis, respectively. The calculated $\boldsymbol{D}_{1\,1\,0}$, $\boldsymbol{D}_{0\,0\,6}$ and $\boldsymbol{D}_{1\,1\,0}/\boldsymbol{D}_{0\,0\,6}$ with the substituted Al^{3+} ion content (x) is also plotted in Fig. 4. The ratio $\boldsymbol{D}_{1\,1\,0}/\boldsymbol{D}_{0\,0\,6}$ is reduced from 1.58 to 1.11 with the Al^{3+} ions content (x) from 0 to 3.0. So that, the $SrAl_xFe_{12-x}O_{19}$ nanofibers grain tends to grow in the preferred direction [0 0 1] and possesses a plate-like morphology, which will be evidenced by the following SEM morphology as shown in Fig. 5.

3.2. Nanofiber morphology

The morphologies of $SrAl_xFe_{12-x}O_{19}$ (x=0.5–3.0) nanofibers with a uniform diameter about 100 nm obtained at 1000 °C for 2 h are shown in Fig. 5. With x increasing from 0.5 to 3.0, the particle morphology basically maintains the plate-like shape except the particle size changed from a large size about 100 nm (Fig. 5a) to a small size about 60 nm (Fig. 5f), whilst the nanofiber morphology varies from the necklace-like (Fig. 5a–d), which is generally linked one-by-one with the plate-like particles, to the structure (Fig. 5e and f) building of multi-particles with a smaller size on the nanofiber cross-section. The nanofiber microstructure so that can be modified by design of the chemical composition.

In order to confirm the chemical composition of the as-prepared $SrAl_xFe_{12-x}O_{19}$ nanofibers, a quantitative elemental analysis on these samples was carried out by the energy-dispersive X-ray spectrometer attached to the scanning electron microscope. Fig. 6 shows the EDX spectra of the $SrAl_xFe_{12-x}O_{19}$ nanofibers, and the corresponding elemental analysis results are presented in Table 1. The results indicate that the atomic percentage (at%) of Sr, Al and Fe in the $SrAl_xFe_{12-x}O_{19}$ nanofibers estimated by EDX basically agree with the designed composition.

3.3. Magnetic properties

It is well known that in a unit cell of M-type ferrite, the Fe^{3+} ions are arranged in five different interstitial sites, three octahedral (2a, 12k, 4f_2), one tetrahedral (4f_1) and one trigonalbipyramid (2b). The spin directions for 2a, 12k and 2b sublattices are parallel to each other (in the direction of the crystallographic c-axis), whereas those of 4f_1 and 4f_2 sublattices are in the opposite

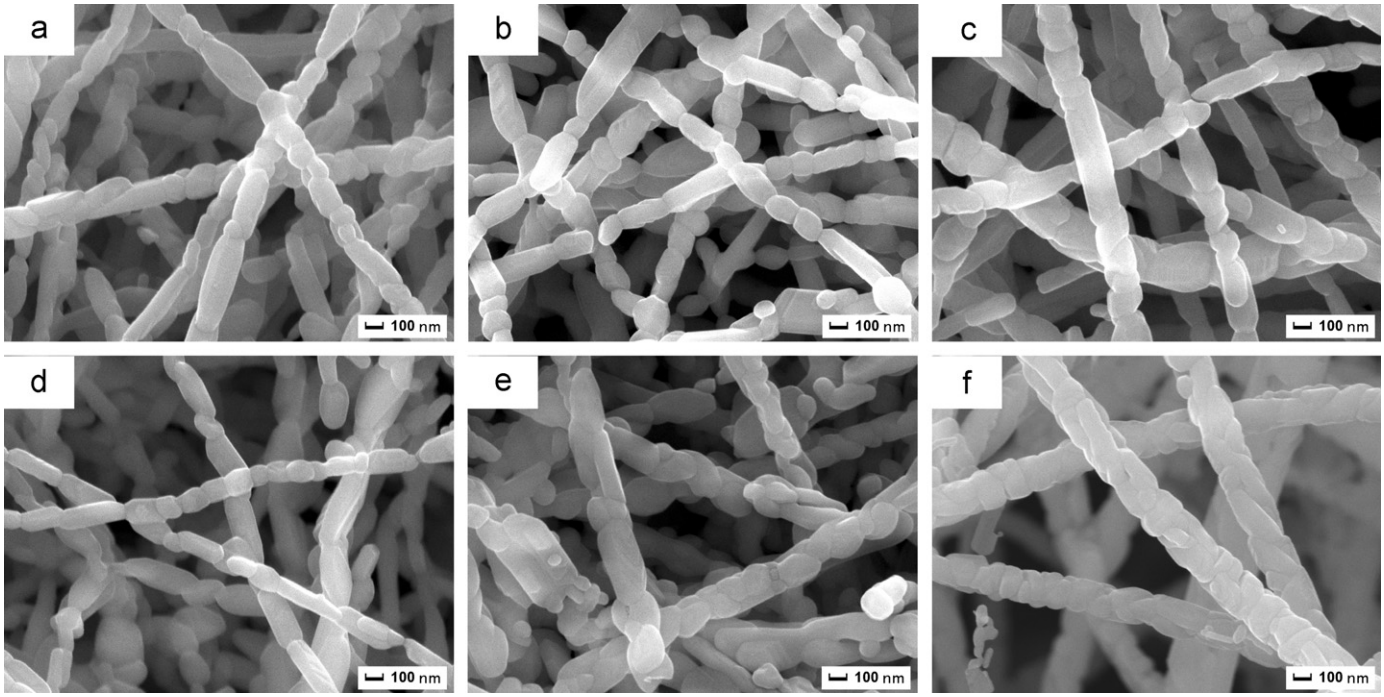

Fig. 5. SEM morphologies of $SrAl_xFe_{12-x}O_{19}$ nanofibers with different Al^{3+} ion contents (***x***): (a) 0.5; (b) 1.0; (c) 1.5; (d) 2.0; (e) 2.5; and (f) 3.0.

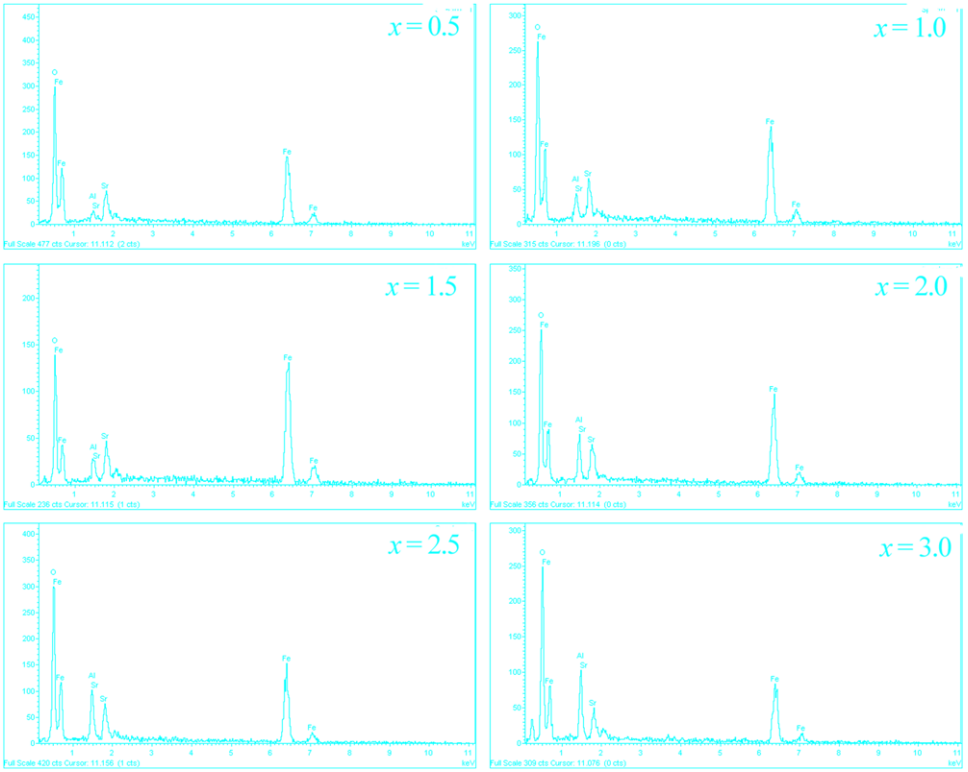

Fig. 6. EDX spectra of $SrAl_xFe_{12-x}O_{19}$ nanofibers with different Al^{3+} ion contents (x).

direction, which are coupled by super-exchange interactions through O^{2-} ions.

Fig. 7 shows the typical hysteresis loops of the randomly oriented $SrAl_xFe_{12-x}O_{19}$ nanofibers measured at the room temperature. From Fig. 7, it can be seen that the Al^{3+} ion substitution has a significant effect on the magnetic properties of the $SrAl_xFe_{12-x}O_{19}$ nanofibers. The coercivity ($\boldsymbol{H_c}$) increases significantly, with values of 452 kA m^{-1}(x=0), 517 kA m^{-1} (x=1.0) and 617 kA m^{-1} (x=2.0), while the magnetization ($\boldsymbol{M_s}$) decreases obviously, with the estimated values 62 A m^2 kg^{-1} (x=0), 42 A m^2 kg^{-1} (x=1.0) and 25 A m^2 kg^{-1} (x=2.0), respectively. Compared to the reported nanoparticles [10] and nano-films [12], the one-dimensional $SrAl_xFe_{12-x}O_{19}$ nanofibers show a similar coercive behavior to the nanoparticles, with a much higher $\boldsymbol{H_c}$ value than for the nano-films as shown in Table 2. These one-dimensional $SrAl_xFe_{12-x}O_{19}$ nanofibers due to a high aspect ratio

can be used as building blocks for future micro- and nano-electromagnetic devices with a tunable ferromagnetic resonant frequency [20,26].

The effect of different Al^{3+} ion contents on $\boldsymbol{M_s}$ value for the randomly oriented $SrAl_xFe_{12-x}O_{19}$ nanofibers calcined at 1000 °C for 2 h measured at room temperature (298 K) and 77 K are plotted in Fig. 8. The magnetization at both room temperature (298 K) and 77 K for these nanofibers shows a continuous reduction with increasing Al^{3+} ion contents, from 62 ($x=0$) to 13 A m^2 kg^{-1} ($x=3.0$) and 85 ($x=0$) to 16 A m^2 kg^{-1} ($x=3.0$) corresponding to 298 and 77 K, respectively. The reduction of $\boldsymbol{M_s}$ with the Al^{3+} ion substitution can be explained on the basis of the magnetic collinearity. For the pure strontium ferrite, the magnetic moments of Fe^{3+} ions are commonly arranged collinearly due to the existence of super-exchange interactions. However, with the non-magnetic Al^{3+} ions entering the lattice, some super-exchange interactions will be suppressed, which causes the magnetic collinearity break down [27]. As a result, the $\boldsymbol{M_s}$ value will decrease with the Al^{3+} ion content. Comparing the estimated $\boldsymbol{M_s}$ values at room temperature and at 77 K in Fig. 8, the $\boldsymbol{M_s}$ value at 77 K is generally larger than the value at room temperature, which can be explained referring Bloch's law [28] expressed as

$$\boldsymbol{M_S}(T) = \boldsymbol{M_S}(0)(1-(T/T_0)^{1.5}) \quad (1)$$

where $\boldsymbol{M_s}(0)$ is the saturation magnetization estimated at 0 K and T_0 is the temperature at which the saturation magnetization is zero, respectively. According to Eq. (1), the $\boldsymbol{M_s}$ value measured at room temperature for the $SrAl_xFe_{12-x}O_{19}$ ($0 \le x \le 3.0$) nanofibers is smaller than the measured at 77 K.

The effect of Al^{3+} ion contents on $\boldsymbol{H_c}$ value for the randomly oriented $SrAl_xFe_{12-x}O_{19}$ nanofibers calcined at 1000 °C for 2 h measured at room temperature (298 K) and 77 K are represented in Fig. 9. For the coercivity, it differs from the $\boldsymbol{M_s}$ behavior and its value initially increases and then decreases with the Al^{3+} ion content both at room temperature and 77 K, and a similar phenomenon was reported by Choi et al. [10]. When x arrives at 2.0, the coercivity gets a maximum value of 617 kA m^{-1} (298 K) and 547 kA m^{-1} (77 K), respectively.

Theoretically, the $SrAl_xFe_{12-x}O_{19}$ nanofiber coercivity is affected by many factors, such as the particle size, morphology,

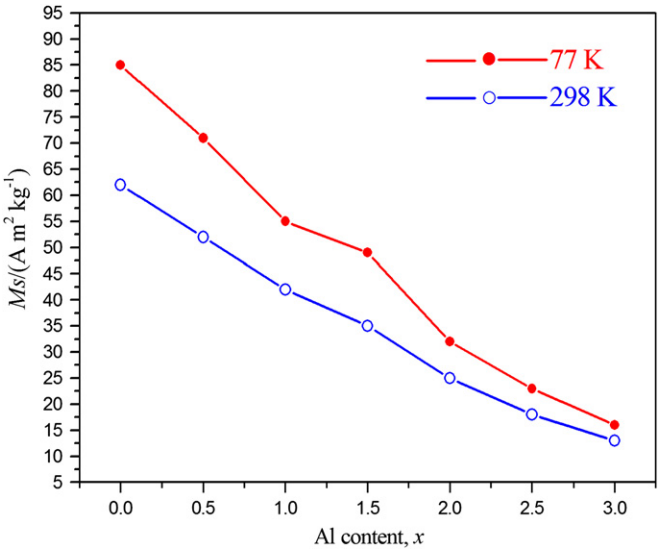

Fig. 8. Magnetization ($\boldsymbol{M_s}$) for $SrAl_xFe_{12-x}O_{19}$ nanofibers measured at room temperature (298 K) and 77 K with different Al^{3+} ion contents (x).

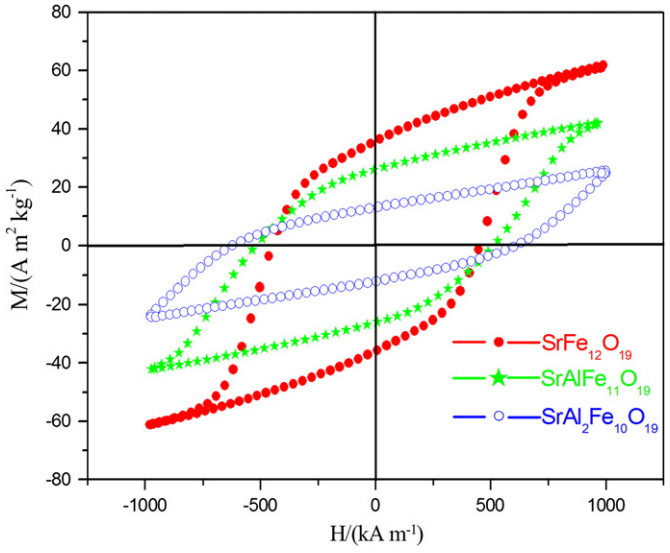

Fig. 7. Typical hysteresis loops of the randomly oriented $SrAl_xFe_{12-x}O_{19}$ nanofibers with different Al^{3+} ion contents.

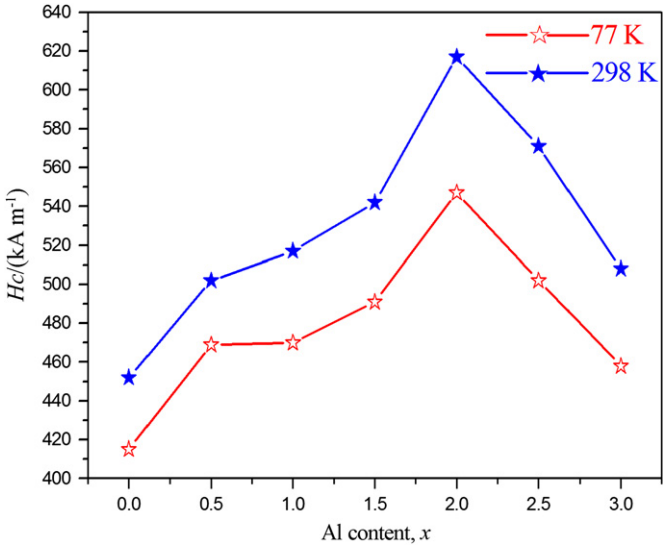

Fig. 9. Coercivity ($\boldsymbol{H_c}$) for $SrAl_xFe_{12-x}O_{19}$ nanofibers measured at room temperature (298 K) and 77 K with different Al^{3+} ion contents (x).

Table 2
Effect of Al^{3+} ion content (x) on coercivity ($\boldsymbol{H_c}$) for various dimensional M-type ferrites derived from different preparative routes.

M-type ferrites	Preparative routes	$\boldsymbol{H_c}$/(kA m^{-1})		
		$x=0$	$x=1.0$	$x=2.0$
$BaAl_xFe_{12-x}O_{19}$ nanoparticles [10]	Sol–gel	406	605	693
$SrAl_xFe_{12-x}O_{19}$ nanofibers (present work)	Electrospinning	452	517	617
$SrAl_xFe_{12-x}O_{19}$ nano-films [12]	Pulse laser ablation deposition	139	215	292

ion substitution, interface structure, strain and crystal defects [29]. Among these factors, the particle size and substitution ion are undoubtedly the two most important as the $SrAl_x$-$Fe_{12-x}O_{19}$ nanofiber grain sizes (37–65 nm) are within the critical single-domain size around 60 nm for the strontium ferrite reported by Lin et al. [30] and Kulkarni et al. [31], as the coercivity will decrease with the particle size reduction when the particle size is within the critical size of single-domain [32]. But, one finds that although the grain size for the $SrAl_xFe_{12-x}O_{19}$ nanofibers exhibits a decrease with the Al^{3+} ion content increase (Fig. 4), the coercivity is clearly increased with the Al^{3+} ion content up to 2.0 (Fig. 9). It means that the effect of the Al^{3+} ion substitution on $\boldsymbol{H_c}$ is much more significant than that of the particle size.

According to the Stoner–Wolfforth model [33], the $\boldsymbol{H_c}$ value can be expressed as

$$\boldsymbol{H_C} \propto \frac{K_1}{\boldsymbol{M_S}} \tag{2}$$

where K_1 is the magnetocrystalline anisotropy constant. $\boldsymbol{H_c}$ is closely related to the anisotropy constant K_1 and saturation magnetization $\boldsymbol{M_s}$. When the substitution ion content x is below 2.0, according to the Mössbauer spectroscopy [5,10] the substitution Al^{3+} ions prefer to occupy the $4f_2$, $2a$, $4f_1$ and $12k$ sites and these substituted Al^{3+} ions only result in a weak decrease of the anisotropy constant [10,34], while the $\boldsymbol{M_s}$ value decrease rapidly. Referring Eq. (2), the $\boldsymbol{H_c}$ value should exhibit an increase when the substituted Al^{3+} ion content x is in the range of 0–2.0. However, when the substituted Al^{3+} ion content x is over 2.0, the coercivity reduction can be primarily be attributed to the significant anisotropy constant decrease arising from some Al^{3+} ions occupying $2b$ site and the particle size reduction [5,10].

Compared to the $\boldsymbol{H_c}$ values measured at room temperature (Fig. 9), the coercivity for the nanofibers measured at 77 K is much lower. As the non-magnetic Al^{3+} ions replace the magnetic Fe^{3+} ions, the magnetic collinearity of strontium ferrite will in some degree break down due to the suppression of the strong tetragonal and octahedral exchange interactions. The entering of non-magnetic Al^{3+} ions and the super-exchange interaction suppression may cause the observed phenomenon in this work. A similar phenomenon for the Sn–Zn substituted barium ferrite nanoparticles was reported by Fang et al. [27]. The complete explanation for this phenomenon needs a further study.

4. Conclusion

The Al^{3+} ions substituted M-type strontium ferrite nanofibers ($SrAl_xFe_{12-x}O_{19}$, $x=0$–3.0) with a diameter of about 100 nm have been prepared by electrospinning and subsequent calcination at 1000 °C for 2 h. The lattice parameters $\boldsymbol{a}$ and $\boldsymbol{c}$ are found to decrease with increasing Al content owing to a smaller ionic radius of Al^{3+} ions compared with that of Fe^{3+} ions and the average grain size reduces from 65 to 37 nm corresponding to the Al^{3+} ion content from 0 to 3.0. With the Al^{3+} ion substitution, the non-magnetic Al^{3+} ions replace the magnetic Fe^{3+} ions, which will suppress the super-exchange interactions, and the magnetization of the nanofibers decreases due to the magnetic collinearity break down. Compared to the value measured at room temperature, the $\boldsymbol{M_s}$ value measured at 77 K has a significant increase, which is in accordance with Bloch's law. However, the coercivity of the $SrAl_xFe_{12-x}O_{19}$ nanofibers initially increases, reaches a maximum value of 617 kA m^{-1} (298 K) and 547 kA m^{-1} (77 K) at $x=2.0$ and then reduces with the Al^{3+} ion content increase further, and this largely arises from the substituted Al^{3+} ion arrangement in different interstitial sites of the strontium ferrite unit cell.

Acknowledgments

This work was financially supported by the National Natural Science Foundation of China (Grant no. 50674048), Research Fund for the Doctoral Program of Higher Education of China (Grant no. 20103227110006) and the Jiangsu Province's Postgraduate Cultivation and Innovation Project (Grant no. CX10B-257Z).

References

[1] S.R. Shinde, S.E. Lofland, C.S. Ganpule, S.M. Bhagat, S.B. Bhagat, S.B. Ogale, R. Ramesh, T. Venkatesan, Appl. Phys. Lett. 74 (1999) 594–596.
[2] N. Chen, K. Yang, M.Y. Gu, J. Alloys Compd. 490 (2010) 609–612.
[3] J. Dho, E.K. Lee, J.Y. Park, N.H. Hur, J. Magn. Magn. Mater. 285 (2005) 164–168.
[4] J.X. Qiu, M.Y. Gu, H.G. Shen, J. Magn. Magn, Mater. 295 (2005) 263–268.
[5] J.X. Qiu, Q.G. Zhang, M.Y. Gu, J. Appl. Phys. 98 (2005) 103905.
[6] T. Kagotania, D. Fujiwara, S. Sugimoto, K. Inomata, M. Homma, J. Magn. Magn. Mater. 272–276 (2004) e1813–e1815.
[7] F. Tabatabaie, M.H. Fathi, A. Saatchi, A. Ghasemi, J. Alloys Compd. 470 (2009) 332–335.
[8] A. Ghasemi, A. Morisako, J. Magn. Magn, Mater. 320 (2008) 1167–1172.
[9] N.J. Shirtcliffe, S. Thompson, E.S. O'Keefe, S. Appleton, C.C. Perry, Mater. Res. Bull. 42 (2007) 281–287.
[10] D.H. Choi, S.W. Lee, S.Y. An, S.I. Park, I.B. Shim, C.S. Kim, IEEE. Trans. Magn. 39 (2003) 2884–2886.
[11] J. Feng, N. Matsushita, T. Murakoso, S. Nakagawa, N. Naoe, J. Magn. Magn. Mater. 193 (1999) 152–154.
[12] O. Heczko, R. Gerber, Z. Šimša, Thin Solid Films. 358 (2000) 206–214.
[13] S. Maensiri, M. Sangmanee, A. Wiengmoon, Nanoscale Res. Lett. 4 (2009) 221–228.
[14] A.M. Morales, C.M. Lieber, Science 279 (1998) 208–211.
[15] L.W. Yin, Y. Bando, Y.C. Zhu, M.S. Li, C.C. Tang, D. Golberg, Adv. Mater. 17 (2005) 213–217.
[16] W.Z. Wang, Y.K. Liu, C.K. Xu, C.L. Zheng, G.H. Wang, Chem. Phys. Lett. 362 (2002) 119–122.
[17] Y.W. Ju, J.H. Park, H.R. Jung, S.J. Cho, W.J. Lee, Compos. Sci. Technol. 68 (2008) 1704–1709.
[18] D. Li, J.T. McCann, Y.N. Xia, M. Marquez, J. Am. Ceram. Soc. 89 (2006) 1861–1869.
[19] J.D. Schiffman, C.L. Schauer, Polym. Rev. 48 (2008) 317–352.
[20] S.K. Nataraj, B.H. Kim, M.D. Cruz, J. Ferraris, T.M. Aminabhavi, K.S. Yang, Mater. Lett. 63 (2009) 218–220.
[21] X.Q. Shen, M.Q. Liu, F.Z. Song, X.F. Meng, J. Sol–Gel Sci. Technol. 53 (2010) 448–453.
[22] M. Sivakumar, A. Gedanken, W. Thong, J. Magn. Magn. Mater. 268 (2004) 182–184.
[23] J. Xiang, X.Q. Shen, F.Z. Song, M.Q. Liu, J. Solid State Chem. 183 (2010) 1239–1244.
[24] Q.S. Zhang, Fundamentals of Inorganic materials Sciences, East China University of Science and Technology Press, Shanghai, 2007.
[25] X.H. He, Q.Q. Zhang, Z.Y. Ling, Mater. Lett. 57 (2003) 3031–3036.
[26] D. Li, Y.L. Wang, Y.N. Xia, Nano. Lett. 3 (2003) 1167–1171.
[27] H.C. Fang, C.K. Ong, X.Y. Zhang, Y. Li, X.Z. Wang, Z. Yang, J. Magn. Magn. Mater. 191 (1999) 277–281.
[28] J.F. Hochepied, M.P. Pileni, J. Appl. Phys. 87 (2000) 2472–2478.
[29] R. Shanker, J. Mater. Sci. 25 (1990) 2465–2570.
[30] C.S. Lin, C.C. Hwang, T.H. Huang, G.P. Wang, C.H. Peng, Mater. Sci. Eng B. 139 (2007) 24–36.
[31] S.D. Kulkarni, S.R. Sainkar, S.K. Date, Appl. Phys. Lett. 68 (1996) 3491.
[32] X.Q. Shen, J. Xiang, F.Z. Song, M.Q. Liu, Appl. Phys A. 99 (2010) 189–195.
[33] P.E. Kazin, L.A. Trusov, D.D. Zaitsev, Y.D. Tretyakov, M. Jansen, J. Magn. Magn. Mater. 320 (2008) 1068–1072.
[34] Y. Xu, G.L. Yang, D.P. Chu, H.R. Zhai, Phys. Status Solidi B 157 (1990) 685–693.